ELSEVIER

A B-spline-based approach to heterogeneous objects design and analysis

Pinghai Yang, Xiaoping Qian*

Department of Mechanical, Materials and Aerospace Engineering, Illinois Institute of Technology, Chicago, IL, 60616, United States

Abstract

The recent advancement of solid freeform fabrication, design techniques and fundamental understanding of material properties in functionally graded materials has made it possible to design and fabricate multifunctional heterogeneous objects. In this paper, we present an integrated design and analysis approach for heterogeneous object realization, which employs a unified design and analysis model based on B-spline representation and allows for direct interaction between the design and analysis model without laborious meshing operation. In the design module, a new approach for intuitively modelling of multi-material objects, termed *heterogeneous lofting*, is presented. In the analysis module, a novel *graded B-spline finite element* solution procedure is described, which gives orders of magnitude of better convergence rate in comparison with current methods, as demonstrated in several case studies. Further advantages of this approach include simplified mesh construction, exact geometry/material composition representation and easy extraction of an isomaterial surface for manufacturing process planning.
© 2006 Elsevier Ltd. All rights reserved.

Keywords: Integrated design and analysis; Heterogeneous object model; Functionally graded materials; B-spline finite element; Material composite representation

1. Introduction

Heterogeneous objects (known as functionally graded materials) are composed of different constituent materials and can exhibit continuously varying material composition and/or microstructure, thus producing gradation in their properties. Heterogeneous objects often possess better mechanical, thermal or electrical performances when compared with the traditional homogeneous objects [1–4]. Moreover, heterogeneous objects can fulfill the critical functional requirements since they can synthesize different properties and various advantages of multiple materials into one monolithic component. In addition, heterogeneous objects can resolve traditional material limitations such as material incompatibility (stress concentration, non-uniform thermal expansion etc.). Due to all the above advantages, heterogeneous objects are being adopted in the design of high efficiency engines, ceramic turbine components, biomaterials, mould and die tools for industrial use, armour and armament components [4–6].

The wide application of heterogeneous objects necessitates a need for using a computer model to represent them.

Various representation schemes, each with its pros and cons, have been proposed [3]. For example, the recent researches on heterogeneous object modelling show that B-spline-based method has excellent representation coverage due to the large number of control points [6,7]. On the other hand, the large degrees of freedom make it inconvenient to edit the model. Hence, an intuitive and efficient heterogeneous object modelling method is needed for designing a B-spline-based heterogeneous object model, which could alleviate the inconvenience induced by the large number of design variables [6,8].

Based upon the computerized object model, finite element methods are often used to analyze these objects [1,9–11]. In homogeneous objects, such analysis typically involves lengthy analysis model setup time, i.e. mesh construction, mesh refinement, boundary condition setup and so on. It is estimated that analysis model setup takes more than 80% of the overall analysis time. In the context of heterogeneous object analysis, this issue is further exacerbated. Besides geometry discretization, material composition also needs to be approximated. Moreover, the separation of design and analysis model makes the design and analysis iteration more complicated.

Therefore, in this paper, we present an integrated design and analysis approach for heterogeneous objects based on

---

* Corresponding author. Tel.: +1 312 567 5855.
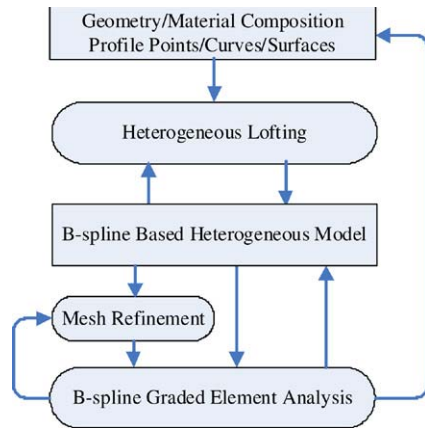*E-mail addresses:* yangpin@iit.edu (P. Yang), qian@iit.edu (X. Qian).

Fig. 1. Flowchart of the integrated design and analysis system.

B-spline representation. It allows efficient heterogeneous object modelling, facilitates the information flow between heterogeneous object design and analysis and leads to orders of magnitude better analysis efficiency. The salient features of this approach include:

- A new *heterogeneous lofting* method is developed to easily and intuitively create the B-spline heterogeneous object model through a set of profile curves/surfaces, which is analogous to the surface lofting method for free form surface modeling in current CAD systems. Meanwhile such a lofting method makes it easy to extract iso-material composition surfaces for manufacturing process planning.
- An *inherent mesh* is defined in the parametric domain by the knot vector(s) of the B-spline representation. Hence the costly and time consuming preprocessing procedure of finite element analysis has been simplified. Furthermore other problems induced by the usual mesh construction process, such as inaccurate geometry and material approximation, are eliminated.
- A novel *graded B-spline finite element* method is developed, which admits a material property gradient at the element level. The material composition accuracy at each element improves the performance of finite element analysis in terms of convergence rate. Hence, the graded B-spline element runs much faster than the traditional Lagrange element in finite element analysis.

Fig. 1 illustrates the structure and the internal information flow of our integrated design and analysis system, in which B-spline unifies the geometry and material composition representation, finite element mesh and shape function in finite element analysis. Such unification leads to efficient information flow from design to analysis without laborious manual meshing operation, which also makes the automation of design optimization possible.

The rest of the paper is organized as follows. In Section 2, we provide a review of current literature. In Section 3, we introduce B-spline as our underlying representation of heterogeneous objects. In Section 4, we present a *heterogeneous lofting* method for modelling geometry and material variation in heterogeneous objects. In Section 5, we propose a *graded*

B-spline finite element method for the analysis of heterogeneous objects. After presenting several case studies to illustrate the whole integrated design and analysis process in Section 6, we conclude this paper in Section 7.

2. Literature review

Various heterogeneous modelling schemes have thus far been proposed to support the creation of geometry as well as the graded material inside. A recent survey on these heterogeneous object modelling methods is available at [3]. Here, we briefly present some prior work that is closely related to our work. An r-m sets-based method is proposed in [12], which handles heterogeneous objects by using r-sets as the basis of representing the geometry and material distribution. A mesh based method is reported in [13,14], which employs four-node iso-parametric quadrilateral elements to model the material distributions. An implicit function-based method is proposed in [15,16] which parameterizes the space by distances from the material features. A B-spline-based method is presented in [1, 6,17,18], which models the object heterogeneity by specifying values of a set of control points and interpolating them with the B-spline shape function. Besides the above approaches, some more approaches are reported, such as the level set-based method [4] and the trivariate simplex splines-based method [19].

Meanwhile, numerous studies have been performed in the analysis of heterogeneous objects. A shape optimization scheme is developed in [9] to design axis symmetrical FGM structures. A domain integral method is used in [20] for calculating stress intensity factors of FGMs. A meshless method is presented in [21] for calculating the fracture parameters of a stationary crack in FGM with arbitrary geometry. A graded element method is proposed in [10] for isotropic and orthotropic FGM analysis under various loading conditions.

Although there are many heterogeneous object modelling and analysis schemes available, serious issues remain, including: design model and analysis model separation, geometry discretization, material composition discretization and so on. In this paper, we propose a B-spline-based integrated design and analysis system for heterogeneous objects, which can reduce the costs induced by the separation of design and analysis model. A similar approach limited in the *homogeneous* object domain was reported in [22,23]. Our approach differs from it in two important aspects: (a) we use *heterogeneous* lofting to create B-spline-based *heterogeneous* object model; (b) we develop a novel graded B-spline finite element method for efficient finite element analysis.

3. B-spline representation for heterogeneous objects

B-splines have been widely used in computer aided design and computer graphics community, which are comprehensively described in CAD and computer graphics literature [24]. In this paper, B-spline representation is used to represent both geometry and material composition of heterogeneous objects.

It is also extended to represent other physical properties of heterogeneous objects [6], which are independent from the material composition, such as temperature field.

Generally speaking, if a heterogeneous object is composed of n_2 different materials and attached with n_3 different physical properties, the modelling space of heterogeneous solid can be denoted as the tensor product of n_1 dimensional geometry space E^{n_1}, n_2 dimensional material space M^{n_2} and n_3 dimensional property space IE^{n_3}.

3.1. Heterogeneous B-spline curve

Given a set of n control points, we can obtain the components of the piece-wise polynomial B-spline curve $\mathbf{C}(u)$ by taking the linear combination of the basis functions weighted by the components of control points, so:

$$\mathbf{C}(u) = \sum_{i=0}^{n} N_{i,p}(u)\mathbf{p}_i$$

where $\mathbf{p}_i \in E^{n_1} \times M^{n_2} \times IE^{n_3}$ are control points for the heterogeneous B-spline curve. $N_{i,p}(u)$ are the pth degree B-spline functions, which are defined as:

$$N_{i,0}(u) = \begin{cases} 1 & \text{if } u_i \leq u \leq u_{i+1} \\ 0 & \text{otherwise} \end{cases}$$

$$N_{i,p}(u) = \frac{u - u_i}{u_{i+p} - u_i} N_{i,p-1}(u) + \frac{u_{i+p+1} - u}{u_{i+p+1} - u_{i+1}} N_{i+1,p-1}(u)$$

where $\mathbf{U} = \{u_0, u_1, \ldots, u_{n+p+1}\}$ is the knot vector. If $n_1 = 2$, this B-spline curve $\mathbf{C}(u)$ presents a 2D heterogeneous curve; If $n_1 = 3$, this B-spline curve $\mathbf{C}(u)$ presents a 3D heterogeneous curve.

3.2. Heterogeneous B-spline tensor surface and solid

By means of tensor products, B-spline surfaces can be constructed starting from a bidirectional net of $(n+1) \times (m+1)$ control points and knot vectors:

$$\mathbf{S}(u, v) = \sum_{i=0}^{n} \sum_{j=0}^{m} N_{i,p}(u) N_{j,q}(v)\mathbf{p}_{i,j}.$$

Then we obtain a bivariate surface over the two independent parameters u and v, where $\mathbf{p}_{i,j}$ are control points of the heterogeneous surface. $N_{i,p}(u)$ and $N_{j,q}(v)$ are the p-th degree and q-th degree B-spline basis functions defined in u and v directions respectively.

Similarly, a tri-variate B-spline volume can also be constructed by means of tensor products:

$$\mathbf{M}(u, v, w) = \sum_{i=0}^{n} \sum_{j=0}^{m} \sum_{k=0}^{l} N_{i,p}(u) N_{j,q}(v) N_{k,r}(w)\mathbf{p}_{i,j,k} \quad (1)$$

where the definition of control points $\mathbf{p}_{i,j,k}$ and B-spline basis functions $N_{i,p}(u)$, $N_{j,q}(v)$ and $N_{k,r}(w)$ are similar to the bivariate B-spline surface, which are defined by the knot vectors of $\mathbf{U} = \{u_0, u_1, \ldots, u_{n+p+1}\}$, $\mathbf{V} = \{v_0, v_1, \ldots, v_{m+q+1}\}$ and $\mathbf{W} = \{w_0, w_1, \ldots, w_{l+r+1}\}$.

3.3. Representation for material properties of heterogeneous objects

In heterogeneous objects design and analysis, controlling heterogeneous object's properties can be more direct and beneficial in design specification than controlling the material composition [6]. The problem of determining the effective properties of a mixture of materials has been extensively studied [25,26]. Many equations are given to approximate relationships between material properties and material composition in those work. In this paper, for the sake of briefness, we choose a linear rule, which uses a volume-fraction-weighted sum of the material property to predict the property of the composite. For example, suppose a heterogeneous object is composed of two materials. Then we can define the value of the material property as:

$$e = e_1 m_1 + e_2 m_2 \quad (2)$$

where m_1 and m_2 are the volume fraction of the two composite materials at each point, e_1 and e_2 are the property values of these two materials. The B-spline representation for material properties could be derived by combining this material property equation and Eq. (2).

Note, the linear rule (Eq. (2)) is adopted solely for simplicity reason. Other more complex equations, such as inverse rule, can be used as well, where only Eq. (2) needs to be updated for each control point.

4. Heterogeneous object modelling through heterogeneous lofting

In this section, we present our new *heterogeneous lofting* method for modelling geometry and material variation in heterogeneous object modelling, which is analogous to the lofting method for free form surface modelling in current CAD systems. In freeform surface modelling, the homogeneous surface lofting can be defined as follows:

Homogeneous lofting: Given a set of $n + 1$ profile curves $\mathbf{C}_0(u), \mathbf{C}_1(u), \ldots, \mathbf{C}_n(u) \subset E^3$, construct a skinned surface $\mathbf{S}(u, v)$ that passes through all these profile curves. More precisely, we have $\mathbf{S}(u, v_i) = \mathbf{C}_i(u)$ for $0 = v_0 < v_1 < \cdots < v_n = 1$.

The developed heterogeneous lofting method can be derived from homogeneous lofting directly, which is defined as:

Heterogeneous lofting: Given a set of $n + 1$ geometry/material profile features, construct a heterogeneous object passing through both geometry and material compositions of all the profile features. More precisely:

- in univariate heterogeneous lofting, we have $\mathbf{C}(u_i) = \mathbf{q}_i \in E^{n_1} \times M^{n_2} \times IE^{n_3}$ for $0 = u_0 < u_1 < \cdots < u_n = 1$, where $\mathbf{C}(u)$ is the lofted heterogeneous curve, $\mathbf{q}_i$ are heterogeneous profile points;
- in bivariate heterogeneous lofting, we have $\mathbf{S}(u, v_i) = \mathbf{C}_i(u) \subset E^{n_1} \times M^{n_2} \times IE^{n_3}$ for $0 = v_0 < v_1 < \cdots < v_n = 1$, where $\mathbf{S}(u, v)$ is the lofted heterogeneous surface, $\mathbf{C}_i(u)$ are heterogeneous profile curves;
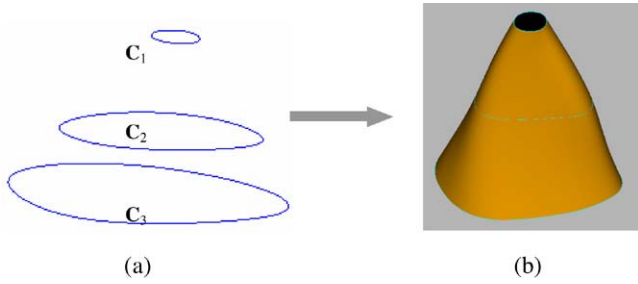
Fig. 2. A typical homogeneous lofting example. (a) Profile curves. (b) Lofted surface.

- in trivariate heterogeneous lofting, we have $\mathbf{M}(u, v, w_i) = \mathbf{S}_i(u, v) \subset E^{n_1} \times M^{n_2} \times IE^{n_3}$ for $0 = w_0 < w_1 < \cdots < w_n = 1$, where $\mathbf{M}(u, v, w_i)$ is the lofted heterogeneous volume, $\mathbf{S}_i(u, v)$ are heterogeneous profile surfaces.

For implementing the homogeneous surface lofting algorithm, we assume that all $n + 1$ profile curves have a common degree p and knot vector $\mathbf{U}$. If not, the common degree elevation and knot insertion algorithms can be used [24]. Then, for the v direction a degree q is chosen, parameters $t_k, k = 0, 1, \ldots, n$, can be calculated, for example, by the chord length method, and a knot vector $\mathbf{U}$ can be computed, for example, by averaging parameters [24]. Suppose $\mathbf{q}_{ij} \in E^3$ is the i-th control point of j-th curve and $\mathbf{p}_{ij} \in E^3$ is the ij-th control point of the lofted surface $\mathbf{S}(u, v)$. The control points of $\mathbf{S}(u, v)$ are computed by solving the following linear equations:

$$
\begin{bmatrix}
1 & 0 & 0 & \cdots & 0 \\
N_{0,q}(t_1) & N_{1,q}(t_1) & N_{2,q}(t_1) & \cdots & N_{n,q}(t_1) \\
N_{0,q}(t_2) & N_{1,q}(t_2) & N_{2,q}(t_2) & \cdots & N_{n,q}(t_2) \\
\vdots & \vdots & \vdots & \ddots & \vdots \\
0 & 0 & 0 & \cdots & 1
\end{bmatrix}
\begin{bmatrix}
\mathbf{p}_{i0} \\
\mathbf{p}_{i1} \\
\mathbf{p}_{i2} \\
\vdots \\
\mathbf{p}_{in}
\end{bmatrix}
$$

$$
=
\begin{bmatrix}
\mathbf{q}_{i0} \\
\mathbf{q}_{i1} \\
\mathbf{q}_{i2} \\
\vdots \\
\mathbf{q}_{in}
\end{bmatrix}
$$

which can be abbreviated as $\mathbf{NP} = \mathbf{Q}$. Hence, we get a lofted surface with degree (p, q), knot vectors $\mathbf{U}$ and $\mathbf{V}$ and control points $\mathbf{P} = \{\mathbf{p}_{ij} \in E^3\}$. An example of modelling a surface with the homogeneous lofting method is shown in Fig. 2.

If we convert modelling space from E^3 to $E^2 \times M^1$, i.e. treating the z coordinates of all the control points as material compositions, we can get the new profile curves shown in Fig. 3(a) from the old ones shown in Fig. 2(a). Then, by applying the same lofting algorithm introduced above, we obtain a 2D heterogeneous surface, as shown in Fig. 3(b). The main difference comes from the physical constraint of the third component (coordinate) in heterogeneous lofting, i.e. it should be a positive value and less than 1, since it means the volume fraction of one material composition.
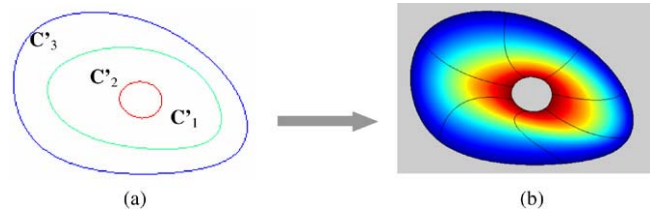

Fig. 3. A typical heterogeneous lofting example. (a) Profile curves. (b) Lofted heterogeneous object.

Fig. 4. A univariate heterogeneous lofting example. (a) Profile points. (b) Lofted heterogeneous curve.

4.1. Algorithms

As discussed in the previous section, we could directly extend current B-spline geometry modelling methods to heterogeneous objects modelling. In uni-variate heterogeneous lofting, we are given a set of points $\mathbf{Q} = \{\mathbf{q}_k \in E^{n_1} \times M^{n_2} \times IE^{n_3}\}, k = 0, \ldots, n$, and we want to interpolate these points with a p-th degree B-spline curve. Reviewing the curve interpolation algorithm in freeform curve/surface modelling, we find that the univariate heterogeneous lofting algorithm is similar to the curve interpolation algorithm. Hence, we extend the univariate heterogeneous lofting algorithm from the curve interpolation algorithm:

Algorithm 1 (*1D Heterogeneous Lofting Algorithm*).

Input: $n + 1$ data points $\mathbf{q}_k \in E^{n_1} \times M^{n_2} \times IE^{n_3}$ and a degree p
Output: A heterogeneous B-spline curve of degree p that passes all data points
Procedure:
　　Computing a set of $n + 1$ parameters $t_0, \ldots, t_n$;
　　Computing the knot vector $\mathbf{U}$;
　　for $i := 0$ **to** n **do**
　　　for $j := 0$ **to** n **do**
　　　　Evaluating into row i and column j of matrix $\mathbf{N}$;
　　　end
　　end
　　for $k := 0$ **to** n **do**
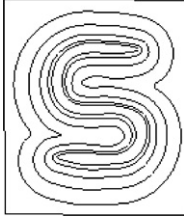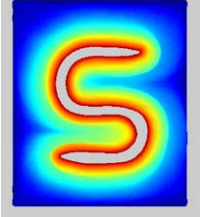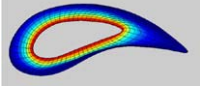　　　Placing data point $\mathbf{q}_k$ on row i of matrix $\mathbf{Q}$;
　　End
　　Using a linear system solver to solve for control points $\mathbf{P}$ from $\mathbf{Q} = \mathbf{NP}$.
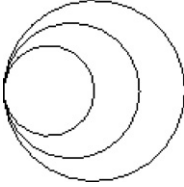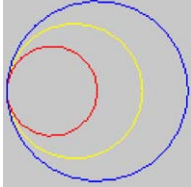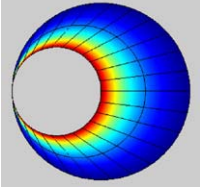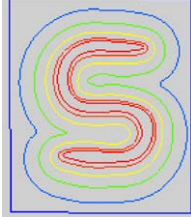
An example of univariate heterogeneous lofting is shown in Fig. 4.

Similarly the bivariate heterogeneous lofting algorithm is an analogy of homogeneous surface lofting. The following

Table 1
Bivariate heterogeneous lofting examples

Index	Profile curves		Lofted surfaces	Description
	Geometry	Material		
Case 1				Design of a heterogeneous surface with a set of iso-material circles.
Case 2				Design of a heterogeneous surface with an S-shaped hole.
Case 3				Design of a section of heterogeneous turbine blade.

algorithm summarizes the required steps for bivariate heterogeneous lofting:

Algorithm 2 (*2D Heterogeneous Lofting Algorithm*).

Input: $n + 1$ heterogeneous B-spline curves
$\mathbf{C}_k \subset E^{n_1} \times M^{n_2} \times IE^{n_3}$
Output: A heterogeneous B-spline surface that passes all input curves
Procedure:
  Computing the unified degree p for input curves $\mathbf{C}_k$ by degree elevating algorithm;
  Computing the unified knot vector $\mathbf{U}$ for input curves $\mathbf{C}_k$ by knot inserting algorithm;
  Defining the degree q in v direction (q < # of curves);
  Computing a set of $n + 1$ parameters $t_0, \ldots, t_n$;
  Computing the knot vector $\mathbf{V}$;
  for $i := 0$ **to** number of control points in u direction **do**
    Retrieving the i-th control points in all input curves $\mathbf{C}_k$;
    Applying uni-variate heterogeneous lofting algorithm on these points to get the i-th column of control points $\mathbf{P}_i$;
  end

Examples implemented using bivariate heterogeneous lofting are illustrated in Table 1.

The trivariate heterogeneous lofting algorithm is also an analogy of homogeneous solid lofting. Hence, the trivariate heterogeneous lofting algorithm can be summarized as:

Algorithm 3 (*3D Heterogeneous Lofting Algorithm*).

Input: $n + 1$ heterogeneous B-spline surfaces
$\mathbf{S}_k \subset E^{n_1} \times M^{n_2} \times IE^{n_3}$
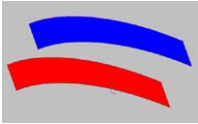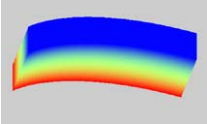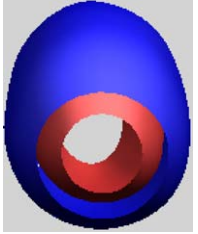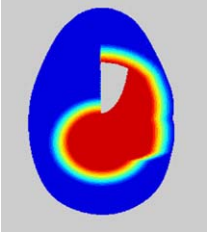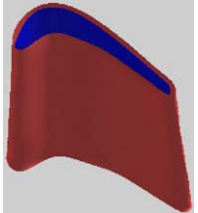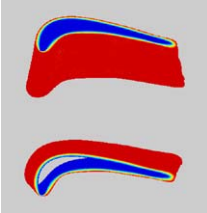**Output:** A heterogeneous B-spline volume that passes all input surfaces
Procedure:
  Computing the unified degree p, q (u, v direction respectively) for input surfaces $\mathbf{S}_k$ by degree elevating algorithm;
  Computing the unified knot vector $\mathbf{U}$, $\mathbf{V}$ for input surfaces $\mathbf{S}_k$ by knot inserting algorithm;
  Defining the degree r in w direction (r < # of surfaces);
  Computing a set of $n + 1$ parameters $t_0, \ldots, t_n$;
  Computing the knot vector $\mathbf{W}$;
  for $i := 0$ **to** number of control points in u direction **do**
    for $j := 0$ **to** number of control points in v direction **do**
      Retrieving the ij-th control points in all input surfaces $\mathbf{S}_k$;
      Applying univariate heterogeneous lofting algorithm on these points to get the ij-th column of control points $\mathbf{P}_{ij}$;
    end
  end

Examples implemented using trivariate heterogeneous lofting are illustrated in Table 2.

Table 2
Trivariate heterogeneous lofting examples

Index	Profile surfaces	Lofted volumes	Description
Case 1			Design of a heterogeneous block.
Case 2			Design of a heterogeneous fuselage body.
Case 3			Design of a heterogeneous turbine blade.

4.2. Homogeneous vs. heterogeneous profile curves/surfaces

4.2.1. Homogeneous material profile curves/surfaces

In previous examples, all of the profile curves/surfaces are composed of constant material compositions. By using these iso-material profile curves/surfaces, the lofted surface/volume possesses a nice feature that all iso-parametric curves/surfaces on the surface/volume are iso-material, which can benefit the process planning in heterogeneous object manufacturing process. Since the iso-material property of the iso-parametric surfaces can be helpful to discretize the whole FGM object into iso-material layers, which is necessary in heterogeneous object fabrication such as powder processing and thermal spraying [27].

4.2.2. Heterogeneous material profile curves/surfaces

However, to make the heterogeneous lofting more flexible, we can bypass this iso-material constraint and use hetero-material profile curves/surfaces, as shown in Table 3. These two examples are corresponding to examples in Table 1. A comparison between these two sets of examples demonstrates the flexibility of heterogeneous lofting in terms of modelling material composition variation.

5. Analysis of heterogeneous objects

In the previous sections, we have presented the B-spline-based model and modelling methods for heterogeneous objects design. Now, we will apply the B-spline finite element analysis based on the same model. Unlike the traditional Lagrange element, B-spline element has an inherent mesh defined by the product of knot vectors. For example, in bivariate B-splines, a mesh is given by $\mathbf{U} \times \mathbf{V}$. These knot spans subdivide the domain into 'elements' (or 'patches' in CAD community).

Another major difference between Lagrange element and B-spline element is the 'node' (or 'control point' in CAD community) distribution. For example, we illustrate this difference between bi-quadratical Lagrange element and uniform biquadratical B-spline element, as shown in Fig. 5. The difference includes: 1. In Lagrange element, the nodal points are on the boundary of the element, which means the element interpolates the nodes; while in B-spline element, this statement is not always valid; 2. In Lagrange element, the neighbour elements only share the nodes on the boundary; while in B-spline element, neighbor elements share more nodes, which results in an elegant feature of higher inter-element continuity. A detail comparison of univariate Lagrange element and B-spline element is presented in Table 4.

5.1. Mesh refinement

Despite all the above differences, there are also many similarities between Lagrange element and B-spline element. For example, the knot insertion operation in B-spline finite element is an analogue of *h*-refinement in Lagrange element, which increases the number of elements but keeps the degree constant; the degree elevation operation in B-spline finite element is an analogue of *p*-refinement in Lagrange element, which increases degree but keeps the number of elements constant. The knot insertion operation and the degree elevation
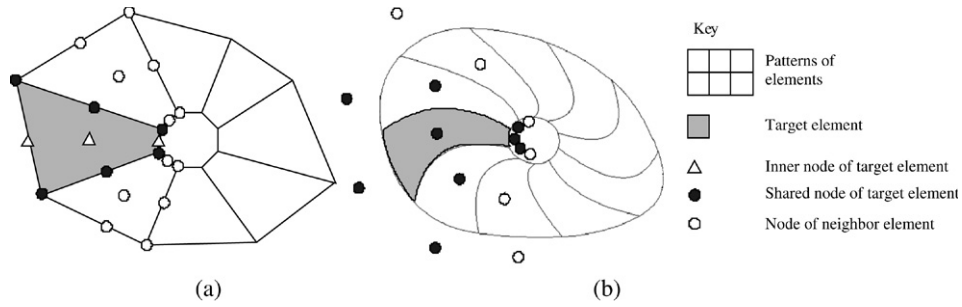
Fig. 5. Comparison of node distribution. (a) Biquadratical Lagrange. (b) Biquadratical B-spline.

Table 3
Heterogeneous lofting examples with hetero-material profile curves

Index	Profile curves		Lofted surfaces	Description
	Geometry	Material		
Case 1				Design of a heterogeneous surface with a set of hetero-material curves.
Case 2				Design of a section of heterogeneous turbine blade with strength at the tip.

Table 4
Comparison of univariate Lagrange element and B-spline element

Items	Quadratical B-spline	Cubic B-spline	Quadratical Lagrange	Cubic Lagrange
Nodes per element	1	1	2	3
Common nodes of neighbour	2	3	1	1
Element continuity	C^1	C^2	C^1	C^2
Inter-element continuity	C^1 or less	C^2 or less	C^0	C^0
Basis interpolates nodal points	No	No	Yes	Yes
Inter-element continuity				
Basis interpolates nodal points				

operation are well-developed techniques in the area of free form surface modelling. For the sake of brevity, we just briefly introduce the basic ideas of these two operations in 1D case. For further investigation, please refer to Piegl's book [24].

In curve knot insertion, a new knot is added into the existing knot vector without changing the curve geometrically or parametrically [24]. Meanwhile, the knot inserting operation will cause a new control point to be added. In most cases,
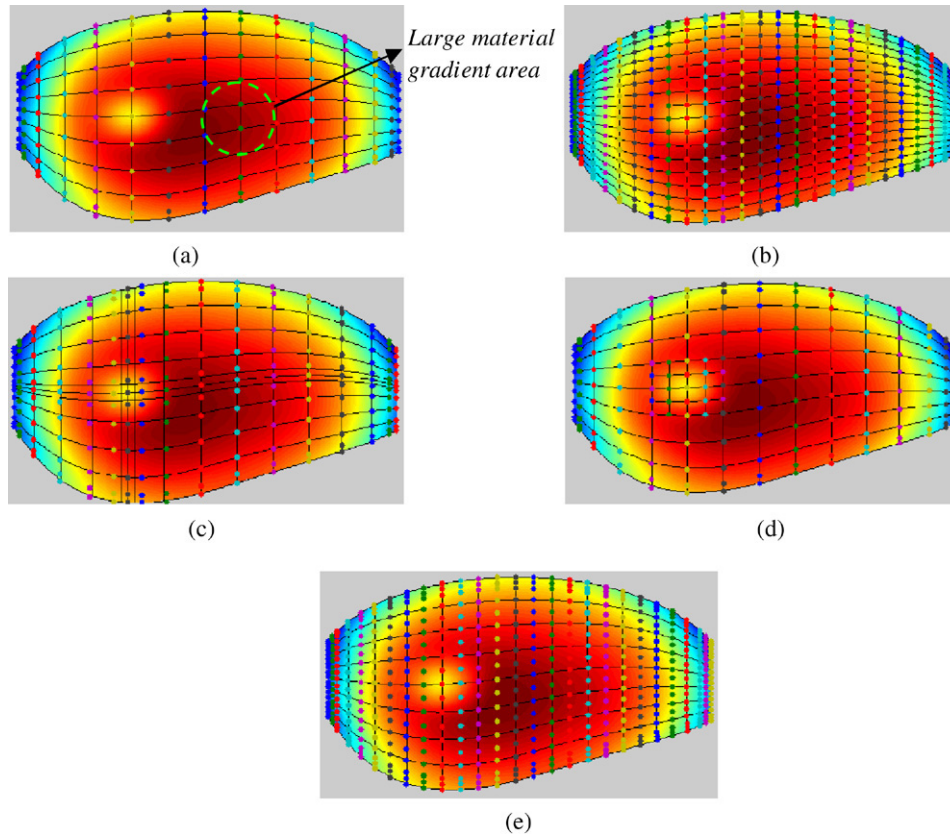
Fig. 6. B-spline element refinement. (a) Initial heterogeneous surface. (b) Uniform knot insertion. (c) Adaptive knot insertion. (d) Hierarchical knot insertion. (e) Uniform degree elevation (control points are denoted by ●).

several existing control points will be removed and replaced with new ones by corner cutting. Given a degree p and a knot vector $\mathbf{U} = \{u_0, u_1, \ldots, u_{n+p+1}\}$, assume a new knot $\bar{u} \in (u_k, u_{k+1}]$ will be inserted. Then the new knot vector can be defined as $\bar{\mathbf{U}} = \{u_0, u_1, \ldots, u_k, \bar{u}, u_{k+1}, \ldots, u_{n+p+1}\}$, and the new $n+1$ control points $\bar{\mathbf{P}} = \{\bar{\mathbf{p}}_0, \bar{\mathbf{p}}_1, \ldots, \bar{\mathbf{p}}_{n+1}\}$ are formed from the original control points $\mathbf{P} = \{\mathbf{p}_0, \mathbf{p}_1, \ldots, \mathbf{p}_n\}$ by:

$$\bar{\mathbf{p}}_i = \alpha_i \mathbf{p}_i + (1 - \alpha_i) \mathbf{p}_{i-1}$$

where

$$\alpha_i = \begin{cases} 1, & i \le k - p \\ \dfrac{\bar{u} - u_i}{u_{i+p} - u_i}, & k - p + 1 \le i \le k \\ 0, & i \ge k + 1. \end{cases}$$

In curve degree elevation, the degree of a B-spline curve is increased without changing the curve geometrically or parametrically. To accomplish this, there is a straightforward algorithm [24], which splits the B-spline curve into Bézier curve pieces, raises the degree of each piece, and then recombines the degree-elevated Bézier curves to produce the new B-spline curve. And the Bézier curve degree elevation algorithm is very simple: Given n-th degree Bézier curve defined by a set of original control points $\mathbf{P} = \{\mathbf{p}_0, \mathbf{p}_1, \ldots, \mathbf{p}_n\}$, the new control points $\bar{\mathbf{P}} = \{\bar{\mathbf{p}}_0, \bar{\mathbf{p}}_1, \ldots, \bar{\mathbf{p}}_{n+1}\}$ can be computed by:

$$\bar{\mathbf{p}}_i = \frac{i}{n+1} \mathbf{p}_{i-1} + \left(1 - \frac{i}{n+1}\right) \mathbf{p}_i \quad 1 \le i \le n.$$

These element refinement procedures (knot insertion and degree elevation) are very important in finite element analysis, which can effectively reduce the local element size. The reduction in element size is helpful to capture the local physical property and improve the element quality, which induce the analysis result converging to the true solution. They are also important for lofting a series of profile curves/surfaces that may be of different degrees or parametrizations.

An implemented example of knot insertion and degree elevation for a 2D heterogeneous object is shown in Fig. 6, which includes the following parts:

- Fig. 6(a) gives an initial bi-cubic B-spline surface with knot spans of 12×8;
- Fig. 6(b) gives the result surface by applying *uniform knot insertion* on the initial B-spline surface, which is still bi-cubic but with knot spans of 24×16;
- Fig. 6(c) gives the result surface by applying *adaptive knot insertion* on the initial B-spline surface, where two new knots of $\bar{u}_1 \in (u_4, u_5]$ and $\bar{u}_2 \in (u_5, u_6]$ are inserted in u direction and two new knots of $\bar{v}_1 \in (v_4, v_5]$ and $\bar{v}_2 \in (v_5, v_6]$ are inserted in v direction. Hence the knot spans become 14×10 but the degrees are kept constant;

- Fig. 6(d) gives the result surface by applying *hierarchical knot insertion* on the initial B-spline surface, which refines each of the central four patches by halving but keeps the degrees constant. Hence in this region, the knot spans is refined from 2×2 to 4×4;
- Fig. 6(e) gives the result surface by applying *uniform degree elevation* on the initial B-spline surface, which is a bi-quartic surface but keeps knot spans constant.

The initial heterogeneous B-spline surface shown in Fig. 6(a) defines both the geometry and material composition of the heterogeneous object. In the analysis process, the initial mesh defined by the knot vectors is not dense enough to obtain a FEM solution with a prescribed accuracy, especially for the spot with large material gradient as shown in Fig. 6(a). To solve this problem, we can apply *uniform knot insertion* as shown in Fig. 6(b). However, this uniform method always induces unnecessary d-o-fs at other areas, which could be significantly reduced by the *adaptive knot insertion* method as shown in Fig. 6(c). But this method still suffers from the local refinement propagating to undesired areas along the knot curves. An alternative is the *hierarchical knot insertion* method as shown in Fig. 6(d), which is to utilize the constraints for the hanging control points to attain the element compatibility [28]. In *degree elevation*, similar methods are used to solve the local refinement problem, as shown in Fig. 6(e).

5.2. Graded B-spline element

In this section, we improve the performance of B-spline element by adopting the concept of graded element used in traditional Lagrange element analysis, which was presented in several previous works [10,11]. We term our new approach as graded B-spline finite element.

In finite element analysis, we interpolate the trial function by the shape functions and the nodal values, which is called finite element approximation. For example, the displacement within an element is defined by the shape functions and the nodal displacements:

$$u = \mathbf{N}_e \cdot \mathbf{u}_e = \sum_{i=1}^{n} N_i u_i$$

where $\mathbf{N}_e$ is the matrix containing the element shape functions, $\mathbf{u}_e$ is the vector containing the local nodal displacements. In our approach, as a benefit of unified B-spline representation of geometry and material composition, the element material property distribution can be represented by the same shape functions and nodal properties. For example, the thermal conductivity k could be defined as:

$$k = \mathbf{N}_e \cdot \mathbf{k}_e = \sum_{i=1}^{n} N_i k_i \tag{3}$$

where $\mathbf{N}_e$ is the matrix of element shape functions, $\mathbf{k}_e$ is the vector of thermal conductivities. Since this kind of element has a property variation represented by B-splines, it is termed as graded B-spline element.
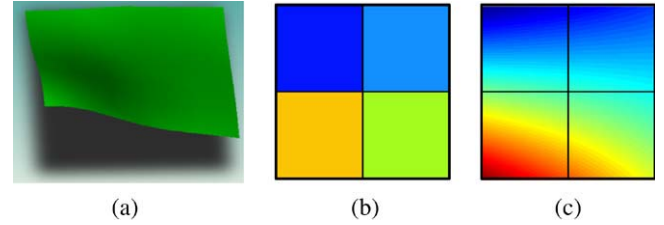

Fig. 7. Homogeneous versus graded finite element. (a) Property height field represented by a rendered surface. (b) Homogeneous element (property value defined by the centroid value). (c) Graded element (property value defined by the weighted sum of nodal values).

In the traditional analysis method for heterogeneous materials, the variational material properties need to be discretized and approximated to an element level. For example, the homogeneous element employs stepwise constant values to approximate the property value, as shown in Fig. 7(b). But in our integrated design and analysis approach, since material property distributions are already represented in B-splines, it does not need to go through a discretization process and can be represented exactly in B-spline element. A comparison of graded B-spline element and widely used homogeneous element is shown in Fig. 7.

We further illustrate this through a heat conduction problem. According to the conservation of energy, the steady heat conduction problem of the above elements is governed by Laplace's equation:

$$\nabla^{\mathrm{T}}(\mathbf{k}\nabla T) = 0 \tag{4}$$

where $\mathbf{k}$ is the thermal conductivity tensor. Then we derive the weak form from Laplace's equation:

$$\int_{\Omega} (\mathbf{K}\nabla T)^{\mathrm{T}} \nabla w \mathrm{d}\Omega = 0. \tag{5}$$

By applying the Galerkin procedure and assuming an isotropic condition, we get a new equation which is a finite element approximation of Eq. (5):

$$\mathbf{w}_e^{\mathrm{T}} \int_{\Omega_e} k \mathbf{B}_e^{\mathrm{T}} \mathbf{B}_e \mathrm{d}\Omega \mathbf{T}_e = 0. \tag{6}$$

In the homogenous element as shown in Fig. 7(b), we use the centroid thermal conductivity value k_e to approximate the value of k, which will bring a discretization error of $e_1 = k - k_e$. Substituting $k = k_e$ into Eq. (6), we have:

$$k_e \mathbf{w}_e^{\mathrm{T}} \int_{\Omega_e} \mathbf{B}_e^{\mathrm{T}} \mathbf{B}_e \mathrm{d}\Omega \mathbf{T}_e = 0. \tag{7}$$

In the graded element, the thermal conductivity is exactly defined by Eq. (3). Substituting Eq. (3) into Eq. (6), we have:

$$\mathbf{w}_e^{\mathrm{T}} \int_{\Omega_e} \mathbf{B}_e^{\mathrm{T}} \mathbf{N}_e \mathbf{K}_e \mathbf{B}_e \mathrm{d}\Omega \mathbf{T}_e = 0. \tag{8}$$

Comparing Eqs. (7) and (8), we can conclude that the graded element is better than the homogeneous element, since the graded element eliminates the discretization error, which exists in the homogeneous element and is harmful to the analysis
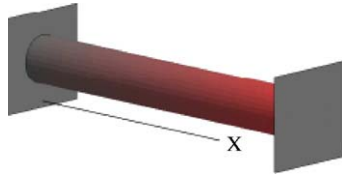
Fig. 8. Cylindrical FEM bar.

Table 5
Mechanical properties of composite materials

Material	Young's modulus (Pa)	Density (kg/m^3)
1	310e9	2000
2	10e9	2000

convergency. We will illustrate the detailed implementation of graded B-spline element in the following section with numerical examples.

6. Approach illustration

6.1. One-dimensional elasticity problem

This one-dimensional elasticity problem is an extension of a similar problem presented in Gosz's FEM book [29]. Here we consider a FGM bar which has a solid circular cross section, as shown in Fig. 8. Let us suppose that the bar has a total length $L = 4$ m and is subjected to the force of gravity acting in the axial direction. And this FGM bar is composed of two primary materials: material 1 and material 2. The mechanical properties of these two materials are given in Table 5:

The Young's modulus distribution of the bar is subjected to the following function:

$$E = x^3 E_1/64 + (1 - x^3/64)E_2.$$

Let us assume that the normal stress distribution on any cross section along the length of the bar is uniform and all points within the bar can displace in the axial direction only. These assumptions make the problem one-dimensional. Applying one-dimensional Hooke's law and strain–displacement relationship yields the following governing function:

$$(E(x)u')' + \rho g = 0 \tag{9}$$

along with two Dirichlet boundary conditions: $u(0) = 0, u(L) = 0$. Solving this ODE with Maple, we can get the exact solution of this problem, as shown in Fig. 9, where the normalized displacement u, is plotted versus the dimensionless length x/L.

To get the graded B-spline element solution, we have the following steps:

Step 1. Specify a set of material feature points as algorithm input, as shown in Fig. 4(a). For every input point $\mathbf{q}_k(x_k, m_k) \in E^1 \times M^1$, m_k is the volume fraction of material 1 at point $\mathbf{q}_k$, which is defined by the material distribution equation.

Step 2. Apply the uni-variate heterogeneous lofting algorithm. Then we get the integrated design and analysis model, i.e. a heterogeneous B-spline curve $\mathbf{C}(u)$, as shown in Fig. 4(b).
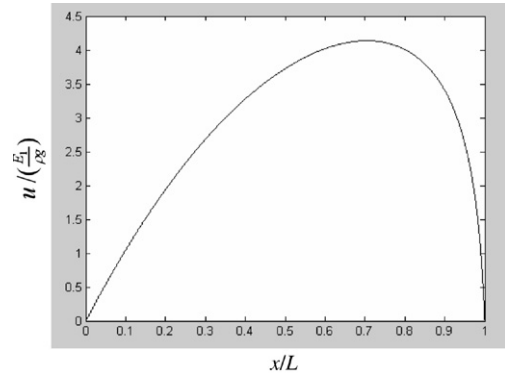

Fig. 9. Exact solution of 1D elasticity.

Step 3. Apply graded B-spline element analysis.

In Step 3, we need to convert the differential equation of Eq. (9) into its weak form, which is mathematically equivalent to Eq. (9), but 2nd order derivative of u has been removed:

$$\int_0^L E(x)u'w'\mathrm{d}x = \rho g \int_0^L w\mathrm{d}x \tag{10}$$

where w is the test function. When plugging the finite element approximations into the weak form of Eq. (10), we have several choices:

1. If we choose homogeneous element method, the Young's modulus of each element is set as a constant: $E(x) = E_i$, where E_i is the Young's modulus at the centroid of the element. Then the finite element approximation of Eq. (10) becomes:

$$\sum_{e=1}^{\text{nel}} E_e \mathbf{w}_e^{\mathrm{T}} \int_0^{l_e} \mathbf{B}_e^{\mathrm{T}} \mathbf{B}_e \mathrm{d}\hat{x} \mathbf{u}_e = \rho g \sum_{e=1}^{\text{nel}} \mathbf{w}_e^{\mathrm{T}} \int_0^{l_e} \mathbf{N}_e^{\mathrm{T}} \mathrm{d}\hat{x}$$

where $\mathbf{N}_e$ is the matrix containing the element shape functions. If $\mathbf{N}_e$ is Lagrange shape functions, the finite element is the traditional Lagrange element; if $\mathbf{N}_e$ is B-spline shape functions, the finite element is the B-spline element;

2. If we choose graded element method, the Young's modulus of each element is interpolated by nodal Young's moduli weighted via shape functions: $E(x) = \mathbf{N}_e \cdot \mathbf{E}_e$. Then the finite element approximation of Eq. (10) becomes:

$$\sum_{e=1}^{\text{nel}} \mathbf{w}_e^{\mathrm{T}} \int_0^{l_e} \mathbf{B}_e^{\mathrm{T}} \mathbf{N}_e \mathbf{E}_e \mathbf{B}_e \mathrm{d}\hat{x} \mathbf{u}_e = \rho g \sum_{e=1}^{\text{nel}} \mathbf{w}_e^{\mathrm{T}} \int_0^{l_e} \mathbf{N}_e^{\mathrm{T}} \mathrm{d}\hat{x}.$$

Similarly, the type of the graded element is defined by the type of shape functions $\mathbf{N}_e$.

Hence, we get four methods of finite element analysis, namely, homogeneous Lagrange element, homogeneous B-spline element, graded Lagrange element and graded B-spline element. In order to compare the convergence rates of these four methods, we employ bi-quadratic elements and calculate the errors of finite element solutions by comparing with the exact solutions. The errors are computed versus the number of d-o-fs, as shown in Fig. 10(a).

In the this paper, we use the number of d-o-fs as a parameter to compare the convergence rate of the finite element analysis
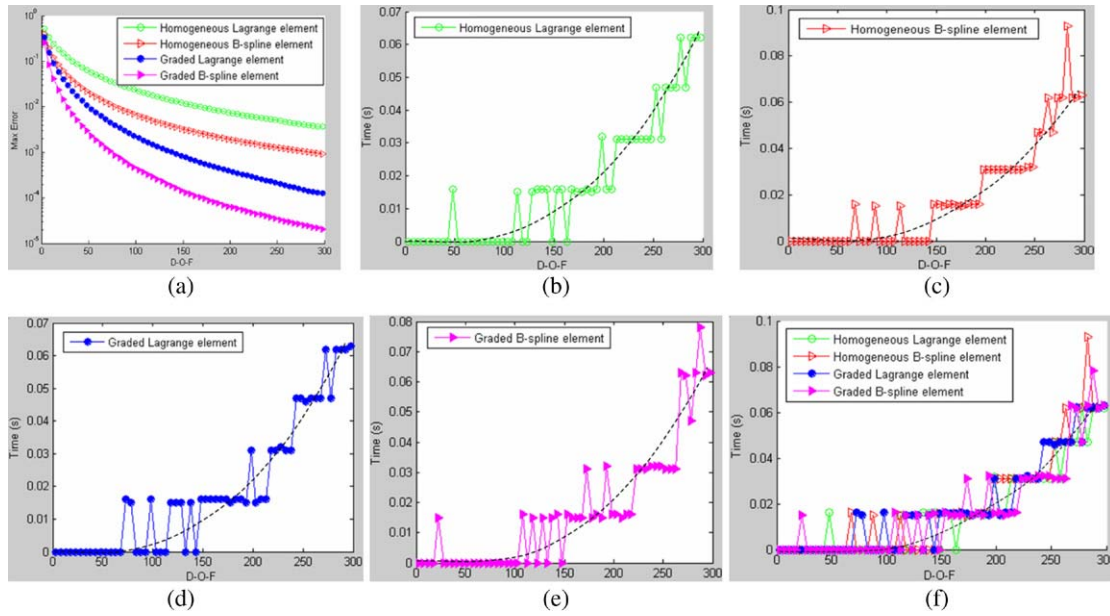
Fig. 10. Comparison of the four methods. (a) Convergence rates. (b) Elapsed time of homogeneous Lagrange element. (c) Elapsed time of homogeneous B-spline element. (d) Elapsed time of graded Lagrange element. (e) Elapsed time of graded B-spline element. (f) Combined elapsed time.

solvers, because it is a good indicator of both the storage and time costs of the solvers. This is shown here both analytically and experimentally. The memory capacity required can be estimated by the amount of memory required to store the entire stiffness matrix, whose size is defined by the number of d-o-fs, for example, if the number of d-o-fs is n, then the size of the stiffness matrix is $n \times n$. And the elapsed time can be estimated from the time for the inverse operation of the stiffness matrix. In our solver, the memory capacity is linear (because of sparse matrix) and the elapsed time is cubic (or less because of sparse LU decomposition) to the number of d-o-fs [30]. To illustrate this, Fig. 10(b)–(e) compare the actual and predicted (dashed line) elapsed time of the four methods separately. For clear identification, Fig. 10(f) combines these four figures together, which shows that the four methods consume approximately same amount of time for the same d-o-fs. Therefore, d-o-fs is a good indicator of convergence efficiency.

From Fig. 10(a), we can find that the graded elements (B-spline and Lagrange) perform much better than the homogeneous elements in terms of convergence rate. Especially, graded B-spline element gives the highest convergence rate, which gains a nearly two order of magnitude better accuracy in comparison with the traditional homogeneous Lagrange element with the same d-o-fs. When d-o-fs equal 300 and the solutions become convergent, the error magnitude of homogeneous Lagrange element is 10^{-2} while that of graded B-spline element is 10^{-4}. Hence, we can conclude that both B-spline and graded element techniques are more efficient than the traditional finite element method.

Also, we make another three experiments by changing the Young's moduli of the two primary materials and the material distribution equation, as shown in Table 6. These results consistently demonstrate that graded B-spline FEM is two orders of magnitude more efficient.
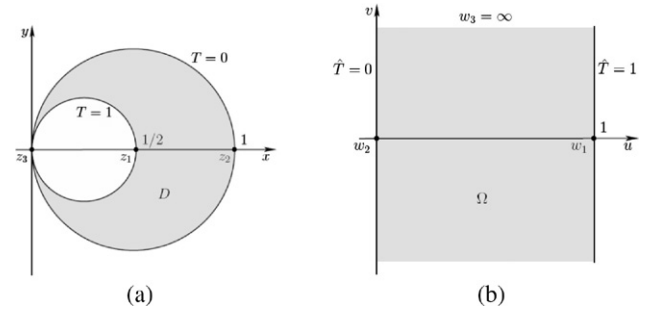

Fig. 11. 2D domains for heat conduction. (a) Domain D before transformation. (b) Domain Ω after transformation.

6.2. Two-dimensional heat conduction problem

In the previous section, we presented a 1D case study to illustrate the detailed procedures of graded B-spline element analysis. In this section, we will extend the graded B-spline element analysis to 2D with higher degrees of shape functions.
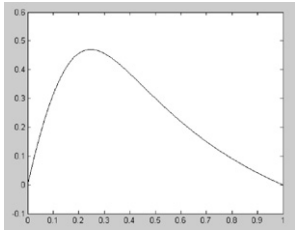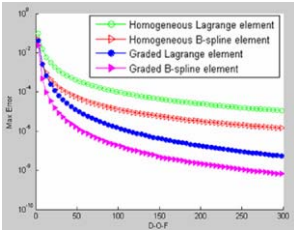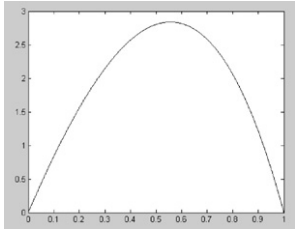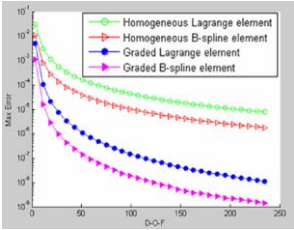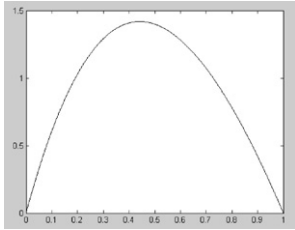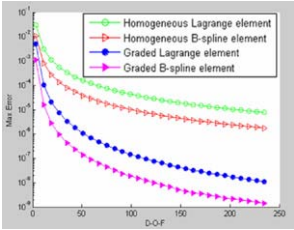
Here we consider a 2D heat conduction problem, and the goal is to determine the temperature distribution due to heat conduction between two isothermal circles that pass through the origin, as shown in Fig. 11(a).

This steady heat conduction problem is governed by Laplace's equation of Eq. (4). The thermal conductivity tensor for this 2D heat conduction problem could be assumed as:

$$\mathbf{k} = \begin{bmatrix} k_x & 0 \\ 0 & k_y \end{bmatrix} \quad k_x = k_y = k_1 e^{\ln(k_2/k_1)(x/(x^2+y^2)-1)}.$$

This property distribution equation is derived from the material distribution equation and Eq. (2). To simplify this problem, we firstly assume that $k_1 = 1$ and $k_2 = e$. Then we use a fractional transformation $w = f(z) = (1-z)/z$ to map the domain D into an infinite strip in the w-plane. Now by solving the new governing function, and transforming the solution back to z-plane, we

Table 6
Summary of several more examples

Index	Exact solution	Comparison of the convergence rates	Description
Case 1			$E_1 = 10e9$ Pa $E_2 = 310e9$ Pa $E = x^3 E_1/64 + (1 - x^3/64)E_2$
Case 2			$E_1 = 20e6$ Pa $E_2 = 10e6$ Pa $E = E_1 e^{\ln(E_2/E_1)x/4}$
Case 3			$E_1 = 10e6$ Pa $E_2 = 20e6$ Pa $E = E_1 e^{\ln(E_2/E_1)x/4}$
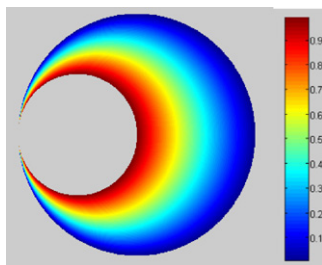
Fig. 12. Exact solution of temperature distribution.

have the analytical solution of the original problem:

$$T(x, y) = \hat{T}(u(x, y)) = (e - e^{-x/(x^2+y^2)})/(e - 1).$$

The temperature contour of this analytical solution is plotted in Fig. 12:

To get the graded B-spline element solution, we will follow the same steps in the 1D elasticity problem. Firstly we apply the bi-variate heterogeneous lofting algorithm to get a heterogeneous surface $\mathbf{S}(u, v)$ as the integrated design and analysis model, as shown in case 1 of Table 1. Notice that we choose rational B-splines instead of B-splines to obtain the geometry of the circles exactly. Following the same process of the 2D steady heat conduction problem in Section 5, we finally get:

$$\sum_{e=1}^{nel} \mathbf{w}_e^{\mathrm{T}} \int_{\Omega_e} \mathbf{B}_e^{\mathrm{T}} \mathbf{N}_e \mathbf{K}_e \mathbf{B}_e \mathrm{d}\Omega \mathbf{T}_e = 0.$$
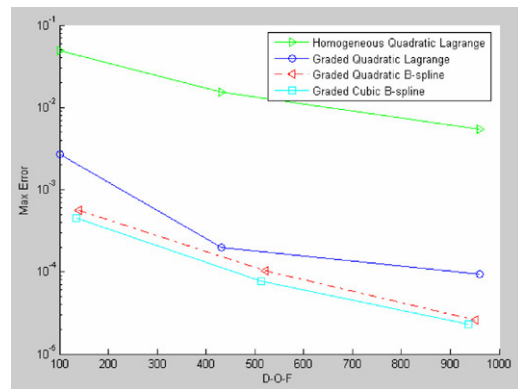

Fig. 13. Comparison of the convergence rates.

After assembling the element matrices and vectors following the usual finite element assembly procedure, the global system of equations can be written simply as $\mathbf{K}_t \mathbf{T} = 0$. Finally, we can get the temperature distribution by solving this equation. Table 7 gives several resulting temperature distributions of finite element analysis with different element types and d-o-fs.

In order to compare the convergence rates of these four methods, we calculate the errors of finite element solutions by comparing them with the exact solutions. The errors are plotted versus the number of d-o-fs, as shown in Fig. 13. The results testify our conclusion that graded B-spline elements give the highest convergence rate, which gains more than two orders of magnitude better accuracy in comparison with the

Table 7
Temperature distributions with different element types and d-o-fs

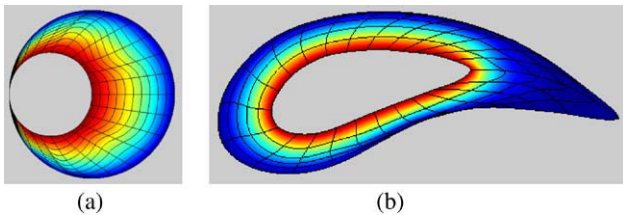| Element type	D-o-fs = 100	D-o-fs = 500	D-o-fs = 1000
Bi-quadratic Lagrange			
Graded bi-quadratic Lagrange			
Graded bi-quadratic B-spline			
Graded bi-cubic B-spline			

(a)　　　　　　(b)

Fig. 14. Temperature distribution of conduction analysis for 2D heterogeneous model in (a) Table 3 case 1, (b) Table 3 case 2.

Fig. 15. Current design without FGM transition.

Table 8
Mechanical properties of composite materials

Material	E (GPa)	ν	α ($10^{-6}/°C$)	k (J/(m °C s))
Ceramic	400	0.22	5	1
Copper	110	0.33	17	400
Titanium	–	–	–	22

homogeneous Lagrange element. And the cubic graded B-spline element performs the best of the four, but only by a small margin in comparison with quadratic graded B-spline element.

Note, the above 1D and 2D results are consistent with results in the algebraic/ experimental comparison of Lagrange element and B-spline element described in [28].

In the above case studies, for the sake of comparison with analytical solutions, we chose examples of relatively simple geometrical shape. However, our approach could be applied to more complicated cases, for example, the applications to the models in Table 3, as shown in Fig. 14.

6.3. Three-dimensional thermal stress problem

In the current design, the cylinder contains an inner copper core and a ceramic coating, as shown in Fig. 15. In the analysis we will assume that the initial (or reference) temperature of this cylinder is 20 °C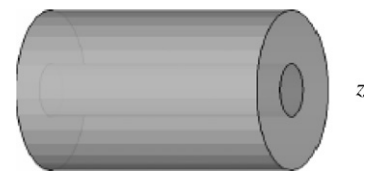, then the inner boundary of the copper core is heated uniformly to a temperature of 200 °C, and outer boundary of the ceramic coating keeps the initial temperature. Hence, there exist thermal stresses, and current research [29] also shows that there exists a sharp discontinuity in the thermal stresses across the interface between copper and ceramic. Now we will redesign this cylinder with FGM to minimize the thermal stresses and remove the discontinuity. The mechanical properties for the copper and ceramic used in the analysis are reported in Table 8.

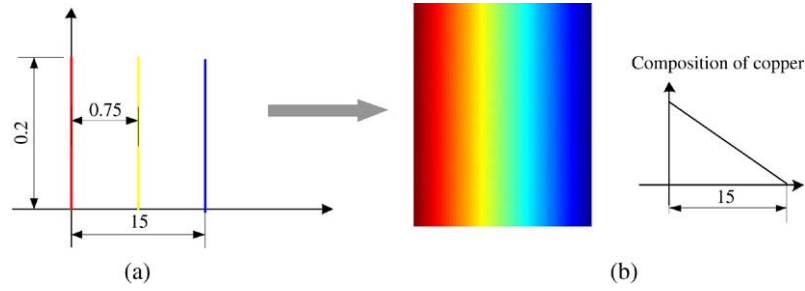Using the axisymmetric property, we can simplify this fully 3D problem to a 2D problem:

Fig. 16. Heterogeneous lofting for modelling the axis section. (a) Profile curves. (b) Lofted heterogeneous surface. (For interpretation of the references to colour in this figure legend, the reader is referred to the web version of this article.)
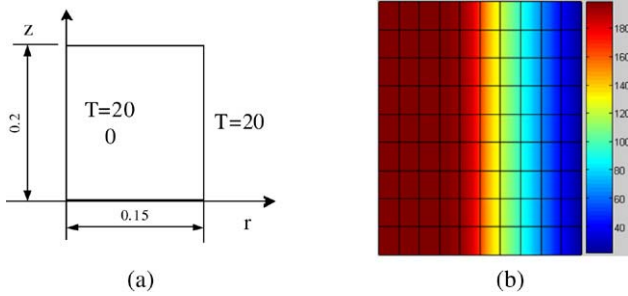

Fig. 17. Heat conduction analysis. (a) Quarter model and associated boundary conditions. (b) Result temperature distribution.

1. In FGM design, instead of designing the material distribution of entire cylinder, we just need to design an axial cross-section.
2. In heat conduction analysis, since the temperature does not vary in the circumferential direction, we reduce the variables in the gradient operator.
3. In thermal stress analysis, we could simplify the Hooke's law.

Step 1. Design the axial cross-section surface of the FGM cylinder by bivariate heterogeneous lofting. To achieve this, we need to create several iso-material profile curves as input for heterogeneous lofting, as shown in Fig. 16. First red line represents pure copper in the core; the second yellow line is the key feature we used to control the material composition; the third blue line represents pure ceramic on the boundary. Now, we set the copper composition m_y of the yellow line as the design variable. Firstly, we choose $m_y = 0.5$, which means that the yellow feature curve contains 50% copper and 50% ceramic. Then applying the bivariate heterogeneous lofting algorithm, we have a heterogeneous B-spline surface as shown in Fig. 16(b).

Step 2. Perform a heat conduction analysis, which will determine the steady-state temperature distribution in the axial cross-section of the cylinder. And then update the heterogeneous surface model by attaching the nodal temperatures to the control points. Since we have assumed that the cylinder is long, it is only necessary to consider the quarter model of the representative section, as shown in Fig. 17(a). Applying the same process as the 2D heat conduction problem presented in the previous section, we finally get the temperature field as shown in Fig. 17 (b):

Step 3. Perform a thermal stress analysis. Due to the absence of body forces, the weak form of the thermal stress problem can be simplified as:

$$\int_{\Omega_e} \mathbf{B}_e^{\mathrm{T}} \boldsymbol{\sigma} \, \mathrm{d}\Omega = 0. \tag{11}$$

Using the axisymmetric property, we can simplify the Hooke's law as:

$$
\begin{Bmatrix} \sigma_{rr} \\ \sigma_{\theta\theta} \\ \sigma_{zz} \\ \sigma_{rz} \end{Bmatrix} = \hat{E}
\begin{bmatrix} 1-\nu & \nu & \nu & \\ \nu & 1-\nu & \nu & \\ \nu & \nu & 1-\nu & \\ & & & \frac{(1-2\nu)}{2} \end{bmatrix}
$$
$$
\times
\begin{Bmatrix} \varepsilon_{rr} - \alpha\Delta T \\ \varepsilon_{\theta\theta} - \alpha\Delta T \\ \varepsilon_{zz} - \alpha\Delta T \\ \gamma_{rz} \end{Bmatrix} = C \cdot
\begin{Bmatrix} \varepsilon_{rr} - \alpha\Delta T \\ \varepsilon_{\theta\theta} - \alpha\Delta T \\ \varepsilon_{zz} - \alpha\Delta T \\ \gamma_{rz} \end{Bmatrix} \tag{12}
$$

where

$$\hat{E} = \frac{E}{(1+\nu)(1-2\nu)}$$

and α is the coefficient of thermal expansion. The quantity ΔT is the temperature change from a stress-free reference state. Applying the concept of graded element, we have:

$$E = \mathbf{N}_e \mathbf{E}_e, \quad \nu = \mathbf{N}_e \boldsymbol{\nu}_e, \quad \alpha = \mathbf{N}_e \boldsymbol{\alpha}_e, \quad \Delta T = \mathbf{N}_e \boldsymbol{\Delta T}_e$$

where $\mathbf{E}_e, \boldsymbol{\nu}_e, \boldsymbol{\alpha}_e$ and $\boldsymbol{\Delta T}_e$ are corresponding nodal property values, for example, $\mathbf{E}_e$ are composed of the Young's moduli of the nodes of element e. Substituting Eq. (12) into Eq. (11), we have:

$$\int_{\Omega_e} \mathbf{B}_e^{\mathrm{T}} \mathbf{C}_e \mathbf{B}_e \, \mathrm{d}\Omega \mathbf{d}_e = \int_{\Omega_e} \mathbf{B}_e^{\mathrm{T}} \mathbf{C}_e \mathbf{N}_e \boldsymbol{\alpha}_e \mathbf{N}_e \boldsymbol{\Delta T}_e \, \mathrm{d}\Omega.$$

Finally, we can get the results for the thermal stress analysis by solving global system. As shown in Fig. 18, the hoop stress changes smoothly in the whole axial cross-section, i.e. the sharp discontinuity across the interface between copper and ceramic has disappeared. And the hoop stress in the ceramic region has been reduced, which will decrease the risk of the fail of the ceramic coating.

To obtain an optimized design of the axial cross-section of the FGM cylinder, we will change the value of the design variable m_y, and run the analysis procedure again, as shown in
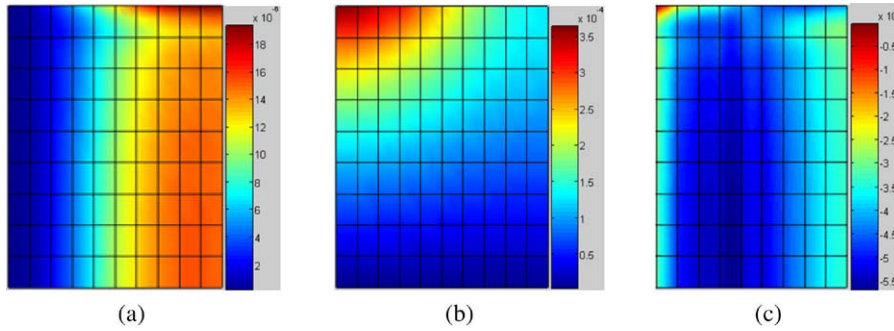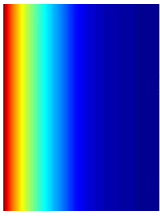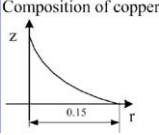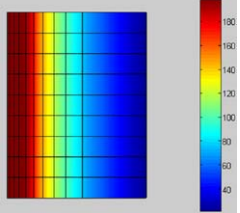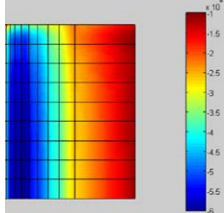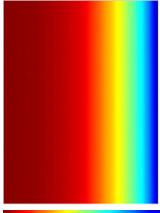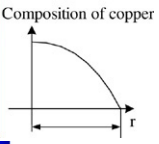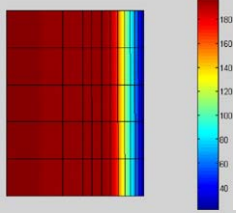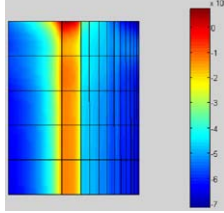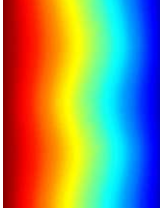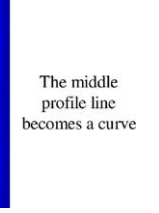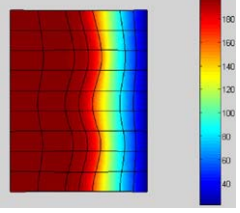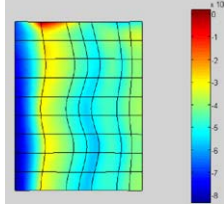
Fig. 18. Results for the thermal stress analysis. (a) Distribution of strain ε_{rr}. (b) Distribution of strain ε_{zz}. (c) Distribution of hoop stress $\sigma_{\theta\theta}$.

Table 9
Summary of other designs

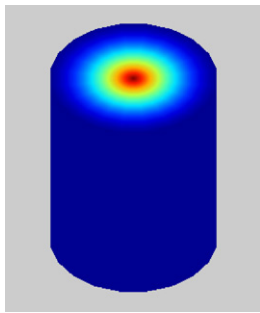| Index	m_y	Heterogeneous object model	Temperature distribution	Hoop stress distribution
Case 1	0.2			
Case 2	0.8			
Case 3	0.5			

Fig. 19. Model of the FGM cylinder.

Table 9. However, the final optimization result depends on the objective functions. For example, if the optimization objective is to minimize the maximum hoop stress, the optimization process will converge at the optimized design with $m_y = 0.61$. Once we get an optimized axial cross-section, we can finally create the FGM cylinder with heterogeneous revolution operation, as shown in Fig. 19.

6.4. Design and analysis of three-dimensional turbine blade

We finish this section with a design and analysis problem of a 3D turbine blade. In this example, the heterogeneous turbine blade is composed of an inner titanium core and a ceramic coating. The mechanical properties for the materials used in the analysis are reported in Table 8. In the analysis for steady-state conduction of this heterogeneous object, we assume that the temperature of the inner and outer boundary surface is 60 °C and 600 °C.

In the design and analysis process, we firstly design three iso-material boundary surfaces of the turbine blade, as shown in Fig. 20(a). Each of the result surfaces is represented by a heterogeneous bi-cubic B-spline surface. Before applying the trivariate heterogeneous lofting algorithm, we need to confirm that all the profile surfaces are compatible. In this example, the outer profile surface defined by a 22×4 control lattice is not compatible with the middle and inner profile surfaces defined 41×8 control lattices, as shown in Fig. 20(b). By
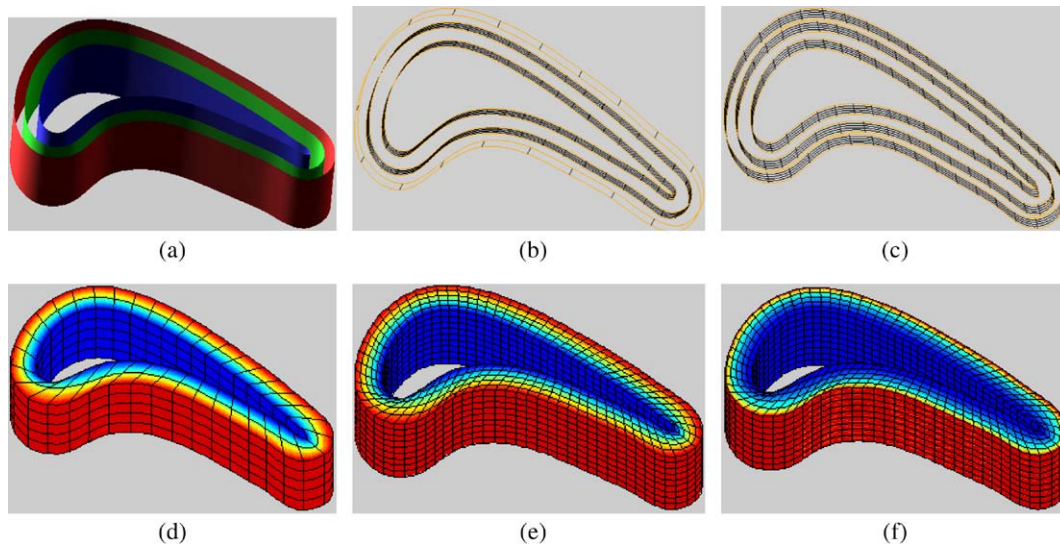
Fig. 20. 3D conduction analysis for heterogeneous turbine blade. (a) Initial profile surfaces in rendered model. (b) Initial profile surfaces in curve mesh model. (c) Refined profile surfaces. (d) Initial heterogeneous model created by heterogeneous lofting. (e) Mesh refinement created by knot inserting. (f) Analysis result of temperature distribution.

using knot insertion, we solve the incompatible problem and unify the degree and knot vector of all profile surfaces, as shown in Fig. 20(c). Then we apply heterogeneous lofting and get an initial heterogeneous volume defined by a $41 \times 8 \times 3$ control lattice (quadratic in w direction), which represents a quadratic transition between both heterogeneous profile surfaces, as shown in Fig. 20(d). To assess convergence of the analysis process, we refine the initial mesh using the knot insertion algorithm, as shown in Fig. 20(e). Finally, we input the refined analysis model into our solver and get the temperature distribution of the turbine blade, as shown in Fig. 20(f). If the analysis result does not converge, we can go back to the mesh refinement module and regenerate the analysis model with enough mesh density or go back to the design module and modify the initial heterogeneous model. All these design and analysis operations are based on the flowchart shown in Fig. 1.

7. Conclusions

In this paper, we presented a B-spline-based approach for heterogeneous object design and analysis, which allows for direct interaction between the design and analysis model. As a benefit of this integrated design and analysis model, the information flow from design model to analysis model has been streamlined, since it does not involve the mesh construction process and the B-spline finite element mesh is directly derived from the design representation. Another benefit is the exact representation of geometry and material distribution in the analysis process.

In the design module, heterogeneous lofting algorithms are introduced to easily and intuitively create heterogeneous object model. Similar to the homogeneous lofting method, this method does not require a grid of control points but a set of profile material features to design the material distribution and/or the geometry of heterogeneous objects. Hence, the design process for heterogeneous object becomes more convenient

than design through B-spline control point specification. Further, such a lofting method makes the extraction of iso-material composition surface relatively straightforward, which is necessary when doing process planning for heterogeneous object manufacturing.

In the analysis module, a novel graded B-spline element solution procedure has been described and validated with case studies. These case studies demonstrated that graded B-spline elements improve the efficiency of finite element analysis up to orders of magnitude better.

The developed approach is based on tensor B-splines and is therefore topologically limited to rectangular shapes. However, our approach is still sufficient for most current heterogeneous objects applications, which are simple in topology. Future research will address such topological limitation.

References

[1] Huang J, Fadel GM. Heterogeneous flywheel modeling and optimization. Journal of Materials and Design 2000;21:111–25 [Invited paper].

[2] Park SM, Crawford RH, Beaman JJ. Volumetric multi-texturing for functionally graded material representation. In: Sixth ACM symposium on solid modeling and applications. 2001. p. 216–24.

[3] Pratt MJ. 3D modelling of material property variation for computer aided design and manufacture. In: Proceedings of the SIAM conference on Mathematics of industry: Challenges and frontiers. 2003. p. 58–83.

[4] Wang MY, Chen SK, Wang X, Mei Y. Design of multi-material compliant mechanisms using level set methods. ASME Transactions: Journal of Mechanical Design 2005;127(5):941–56.

[5] Patil L, Dutta D, Bhatt A, Jurrens K, Lyons K, Pratt M. Representation of heterogeneous objects in ISO 10303 (STEP). In: ASME international mechanical engineering congress and exposition. 2000.

[6] Qian X, Dutta D. Physics-based modeling for heterogeneous objects. ASME Transactions: Journal of Mechanical Design 2003;125:416–27.

[7] Qian X, Dutta D. Feature based design for heterogeneous objects. Computer-Aided Design 2004;36(12):1263–78.

[8] Samanta K, Koc B. Feature-based design and material blending for freeform heterogeneous object modeling. In: Heterogeneous Object Models and their Applications. Computer Aided Design 2005;37(3): 287–305 [special issue].

[9] Hyun SJ, Kim C, Son JH, Shin SH, Kim YS. An efficient shape optimization method based on fem and b-spline curves and shaping a torque converter clutch disk. Finite Elements in Analysis & Design 2004; 40:1803–15.

[10] Kim J, Paulino GH. Isoparametric graded finite elements for nonhomogeneous isotropic and orthotropic materials. ASME Journal of Applied Mechanics 2002;69:502–14.

[11] Santare MH, Lambros J. Use of graded finite elements to model the behavior of nonhomogeneous materials. ASME Journal of Applied Mechanics 2000;67:819–22.

[12] Kumar V, Dutta D. An approach to modeling and representation of heterogeneous objects. ASME Journal of Mechanical Design 1998; 120(4):659–67.

[13] Jackson T. Analysis of functionally graded material representation methods, Ph.D. thesis. Cambridge (MA): Massachusetts Institute of Technology; 2000.

[14] Jackson T, Liu H, Patrikalakis NM, Sachs EM, Cima MJ. Modeling and designing functionally graded material components for fabrication with local composition control. Materials and Design 1999;20(2–3):63–75.

[15] Biswas A, Shapiro V. Approximate distance fields for curves and surfaces. Technical report SAL, 2001-3. University of Wisconsin-Madison, Mechanical Engineering Department, SAL; 2001.

[16] Biswas A, Shapiro V, Tsukanov IG. Heterogeneous material modeling with distance fields. Computer Aided Geometric Design 2004;215–42.

[17] Martin W, Cohen E. Representation and extraction of volumetric attributes using trivariate splines: A mathematical framework. In: Proceedings of the sixth ACM symposium on solid modeling and applications. 2001. p. 234–40.

[18] Wu Z, Seah HS, Lin F. NURBS-based volume modeling. In: International workshop on volume graphics. 1999. p. 321–30.

[19] Hua J, He Y, Qin H. Trivariate simplex splines for inhomogeneous solid modeling in engineering design. ASME Transactions: Journal of Computing and Information Science in Engineering 2005;5(2):149–57.

[20] Gu P, Dao M, Asaro RJ. A simplified method for calculating the crack tip field of functionally graded materials using the domain integral. ASME Journal of Applied Mechanics 1999;66:101–8.

[21] Rao BN, Rahman S. Mesh-free analysis of cracks in isotropic functionally graded materials. Engineering Fracture Mechanics 2003;70(1):1–27.

[22] Hughes TJ, Cottrell JA, Bazilevs Y. Isogeometric analysis: CAD, finite elements, NURBS, exact geometry, and mesh refinement. Computer Methods in Applied Mechanics and Engineering 2005;194:4135–95.

[23] Kagan P, Fischer A, Bar-Yoseph PZ. New B-spline finite element approach for geometrical design and mechanical analysis. International Journal for Numerical Methods in Engineering 1998;41:435–58.

[24] Piegl L, Tiller W. The NURBS book. 2nd ed. New York: Springer-Verlag; 1997.

[25] Markworth AJ, Tamesh KS, Rarks Jr WP. Modeling studies applied to functionally graded materials. Journal of Materials Science 1995;30: 2183–93.

[26] Hashin Z. Analysis of composite materials—A survey. Journal of Applied Mechanics 1983;105:481–505.

[27] Shin KH, Dutta D. Process-planning for layered manufacturing of heterogeneous objects using direct metal deposition. Journal of Computing and Information Science in Engineering 2002;2(4):330–44.

[28] Sabin MA. Spline finite elements. Ph.D. thesis. http://www.damtp.cam.ac.uk/user/na/people/Malcolm. 2000.

[29] Gosz M. Finite element method: Applications in solids, structures and heat transfer. Taylor and Francis CRC Press; 2005.

[30] Press WH, Teukolsky SA, Vetterling WT, Flannerty BP. Numerical recipes in C: The art of scientific computing. 2nd ed. New York: Cambridge University Press; 1992.